Bulletin of the Geological Society of Malaysia, Volume 82, November 2026, pp. 73 - 90
DOI: https://doi.org/10.7186/bgsm82202607

Sedimentological and diagenetic controls on reservoir quality of the Upper Jurassic red beds of the Mangking Sandstones, Tembeling Group, Peninsular Malaysia

Abdulrahman Muhammad[1,2,*], Mohd Suhaili Ismail[1,3], Haylay Tsegab Gebretsadik[4], Abdulrahman Isa Danlami[1], Adamu Kamaliddeen Salisu[1]

[1] Department of Geoscience, Faculty of Science and Information Technology (FSIT), Universiti Teknologi PETRONAS, 32610, Seri Iskandar, Perak, Malaysia
[2] Department of Mineral and Petroleum Resources Engineering, Kaduna Polytechnic, 800282, Kaduna, Nigeria
[3] Shale Gas Research Group (SGRG), Institute of Hydrocarbon Recovery (IHR), Universiti Teknologi PETRONAS, 32610, Seri Iskandar, Perak, Malaysia
[4] Southeast Asia Clastic and Carbonate Research Laboratory, Geoscience Department, Universiti Teknologi PETRONAS, 32610, Seri Iskandar, Perak, Malaysia
*Corresponding author email address: abdulrahmanmuhd1993@gmail.com

Abstract: Red beds sequences have demonstrated potential as hydrocarbon reservoirs in various regions, particularly those located in arid and semi-arid climatic conditions. Understanding the impacts of depositional and diagenetic alterations at different scales is critical to the prediction of reservoir quality distribution and stratigraphic architecture in these deposits. The Jurassic-Cretaceous continental red beds of the Mangking Sandstones in the Tembeling Group, Peninsula Malaysia, have gained attention for their potential as a hydrocarbon reservoir. However, the role of foundational factors (depositional and diagenetic) in reservoir quality assessment of the red beds remains poorly understood. To address this issue, this study employed integrated approaches including field observations, thin section petrography, bulk rock mineralogy (XRD), and grain size analysis to investigate the impact of diagenesis and depositional environment on reservoir quality. The results of this study indicate that the sandstones were deposited in a fluvial-dominated system consisting of mudstone, fine and medium-grained sandstone and conglomerates that are uniformly graded with a preponderance of lithic greywacke owing to the high matrix content. Illitization, quartz overgrowth, compaction, kaolinite formation, pore-filling and grain coating of smectite and the presence of hematite indicate that the sandstones experienced both shallow and deep burial diagenesis. Gravelly and sandy facies exhibit good reservoir quality in comparison to the muddy facies because the impact of cementation was compounded by the high matrix content across all samples (11.33 – 18.00%, avg. 14.63%) with a more pronounced effect in the muddy facies. In general, the sandstones exhibit poor porosity (3.67 – 9.33%, avg. 6.00%) due to intense cementation (high quartz overgrowth) and high matrix contents. However, contribution from micro-fractures (averaging 1.10%) enhances overall porosity and may improve permeability by providing secondary pathways for fluid flow.

Keywords: Depositional environment, diagenesis, Mangking Sandstones, red beds, reservoir quality

INTRODUCTION

Reservoir quality in sandstone formations is primarily governed by two interrelated factors: the original sedimentological framework and the subsequent diagenetic modifications. In red bed successions—continental siliciclastic deposits characterized by pervasive reddish hues due to iron oxide staining—these controls interact in complex and often unpredictable ways, producing highly heterogeneous porosity and permeability distributions (Wang *et al*., 2017; Qiao *et al*., 2020; Adepehin *et al*., 2022; Qian *et al*., 2022; Worden & Utley, 2022; Shahrokhi *et al*., 2024). Although traditionally considered poor reservoir rock due to their high matrix content and extensive cementation, several red bed systems have demonstrated considerable reservoir potential under favorable depositional and diagenetic conditions (Cao *et al*., 2021; Lucero *et al*., 2025).

From a sedimentological perspective, reservoir quality is influenced by grain size, sorting, detrital mineralogy, matrix content, and the energy of the depositional environment. High-energy settings, such as fluvial channels or aeolian dunes, often result in well-sorted, coarser-grained sandstones with higher initial porosity and permeability (Li *et al*., 2020; Wang *et al*., 2021). In contrast, low-energy environments produce finer-grained, poorly sorted deposits that are more susceptible to early pore throat occlusion. Provenance also exerts a first-order control, as sandstones derived from

0126-6187; 2637-109X / Published by the Geological Society of Malaysia.
© 2026 by the Author(s). This is an open access article distributed under the terms of the Creative Commons Attribution (CC-BY) License 4.0.

lithologically diverse or tectonically active source areas may include feldspars and lithic fragments, which are prone to mechanical compaction and chemical alteration (Worden & Burley, 2003; Morad *et al*., 2010; Monsees *et al*., 2021; Bello *et al*., 2025). In red beds, sedimentary facies variability—such as the presence of channels, crevasse splays, and floodplain fines—adds another layer of heterogeneity to initial reservoir properties.

Diagenetic processes—such as mechanical compaction, quartz and carbonate cementation, clay mineral transformations, and dissolution—can significantly enhance or alter the primary pore system. Compaction is typically the dominant porosity-destroying mechanism, especially in deeply buried sandstones or those rich in ductile grains and matrix (Chima *et al*., 2018; Fu *et al*., 2020). Cementation, particularly by quartz overgrowths and early carbonate phases, further occludes primary pores. However, under suitable fluid regimes and burial conditions, dissolution of feldspars and unstable cements may create secondary porosity, which can locally improve reservoir quality (Freiburg *et al*., 2016; Oluwadebi *et al*., 2018; Hosa & Wood, 2020; Favoreto *et al*., 2022; Wadood *et al*., 2024; Yuan *et al*., 2024). The role of authigenic clays—such as chlorite, kaolinite, and illite—is dualistic: they may preserve pore structures by inhibiting quartz cementation or reduce permeability through pore throat bridging (Morad *et al*., 2010).

Additionally, the influence of tectonic history, burial depth, and fluid composition further complicates diagenetic pathways, resulting in a wide variability of red beds reservoir properties (Turner, 1980; Franke & Paul, 1980; Cavaroc & Flores, 1990; Bankole *et al*., 2016; Boukhalfa *et al*., 2025). Collectively, these studies underscore the importance of diagenetic history in determining the hydrocarbon storage and flow potential of red bed reservoirs.

Despite Malaysia's long-standing hydrocarbon exploration and production successes in its offshore basins (i.e., Malay, Sarawak and Sabah Basins), where a growing number of discoveries have been made (Ngah *et al*., 1993; Chakraborty *et al*., 2020; Madon, 2021), the country's inland frontier basins remain significantly underexplored. Among these, the Tembeling Group in Peninsular Malaysia, with over 3000 meters of sedimentary succession including the Mangking Sandstones (containing a red bed sequence) (Koopmans, 1968), has gained attention as an exploration target. Located near the Malay Basin and sharing geological continuity with eastern Peninsular Malaysia, the Mangking Sandstones (approximately 800 meters thick) may hold potential for both hydrocarbon reservoir and storage site for CO_2 sequestration (Ngah *et al*., 1993).

In this study, several research questions are addressed, such as: what are the primary depositional environments represented by the Mangking Sandstones, and how do these environments, whether fluvial or lacustrine, relate to reservoir heterogeneity and quality? How do variations in grain size, sorting, and sedimentary facies affect the distribution of porosity and what sedimentary structures are preserved that might influence fluid flow pathways? The study also investigates key diagenetic processes that have impacted the Mangking Sandstones, including the identification and role of cements such as silica and hematite, and how they contribute to either porosity preservation or reduction. The source of porosity-enhancing features, such as feldspar or lithic grain dissolution, is also examined, along with the extent to which secondary porosity develops.

Based on analytical techniques such as thin section petrography, bulk rock mineralogy (X-ray Diffraction) and grain size analysis, this study aims to characterise the sedimentological features of the Mangking Sandstones, including grain size, composition, and depositional environment and to evaluate their influence on reservoir quality. It also attempts to analyse diagenetic alterations such as cementation, dissolution, and compaction, with a focus on understanding their impact on porosity and permeability.

Geological setting

The study area is situated within the Mangking Sandstones, a subunit of the Tembeling Group, which forms part of the Central Belt of Peninsular Malaysia (Figure 1A & B). This belt represents a segment of the Sukhothai Arc terrane that was accreted during the closure of the Paleo-Tethys Ocean in the Triassic (Metcalfe, 2013; Otofuji *et al*., 2017). During the Permian–Triassic, Peninsular Malaysia experienced the final amalgamation of two major crustal blocks: the Sibumasu Terrane (Western Belt) and the Sukhothai Arc (Central and Eastern Belts), with the Bentong-Raub Suture Zone marking the former boundary of the Paleo-Tethys Ocean.

Following this collisional event, the area underwent significant crustal thickening, foreland basin development, and regional uplift, which subsequently gave rise to the widespread deposition of continental red beds during the Late Triassic (Ng *et al*., 2015; Chung *et al*., 2023). These red beds were primarily formed under semi-arid to tropical subhumid climatic conditions, where alternating wet and dry periods, coupled with well-drained oxidizing environments, promoted the oxidation of iron-bearing minerals such as hematite, imparting the characteristic red coloration to the sediment (Metcalfe, 2013). Such climatic regimes, especially in the context of post-orogenic continental settings, are crucial for understanding the geochemical conditions that favored red bed development.

The Tembeling Group, including the Mangking Sandstone, was deposited in a post-collisional intracratonic setting, with sediments derived from the uplifted Main Range and other pre-existing highlands (Khoo, 1977; Azmi, 2021; Chung *et al*., 2023). These deposits overlie Palaeozoic marine successions and were developed in response to post-orogenic uplift and continental sedimentation that followed the Indo-Sibumasu collision.

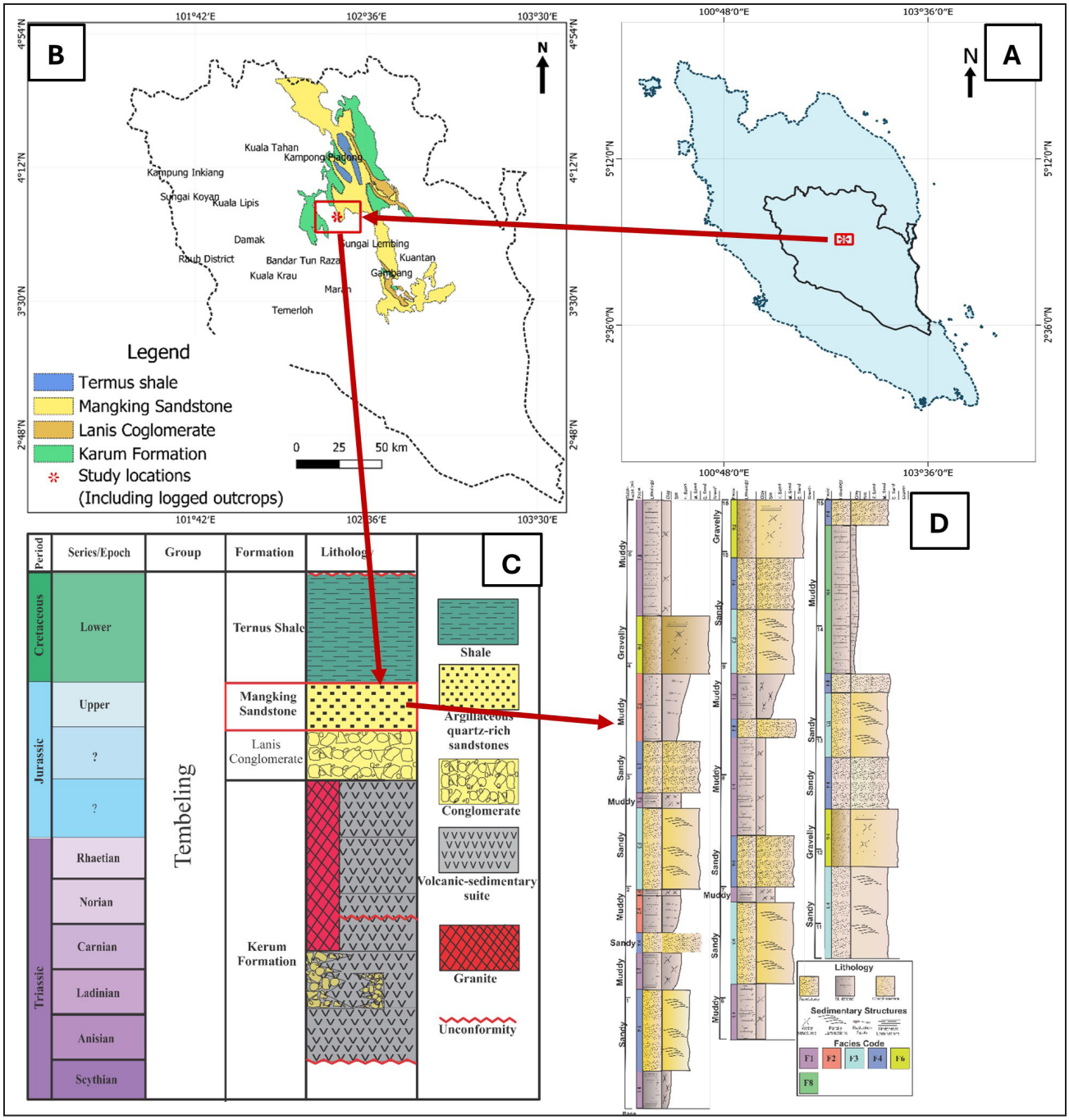


Figure 1: Overview of the geology and stratigraphy of the Tembeling Group. A) and B) location map of the Peninsula, Malaysia. (C) stratigraphy of the Tembeling Group from the Triassic to Cretaceous periods (modified from Azmi *et al*., 2020) and, (D) sedimentary log of the Mangking Sandstones.

The Mangking Sandstones, first described by Khoo (1983) at its type locality along the Mangking River, is composed of interbedded argillaceous rocks and quartz-rich sandstones (Figure 1C). These sandstones exhibit a fining-upward sequence along with features such as tabular and trough cross-bedding. Notably, the plant fossil *Gleichenoides gagauensis* has been identified within the formation, which is dated to the Jurassic–Late Cretaceous period (Khoo, 1977). The formation has an estimated thickness ranging from 600 to 800 meters (Khoo, 1977; Harbury *et al*., 1990). Meanwhile, the Termus Shale, also introduced by Khoo (1983) and named after the Termus River, is the youngest unit within the Tembeling Group. It primarily comprises red ferruginous mudstone and siltstone, with lesser amounts of red shale, sandstone, and breccia, and is estimated to be 300 to 500 meters thick (Harbury *et al*., 1990).

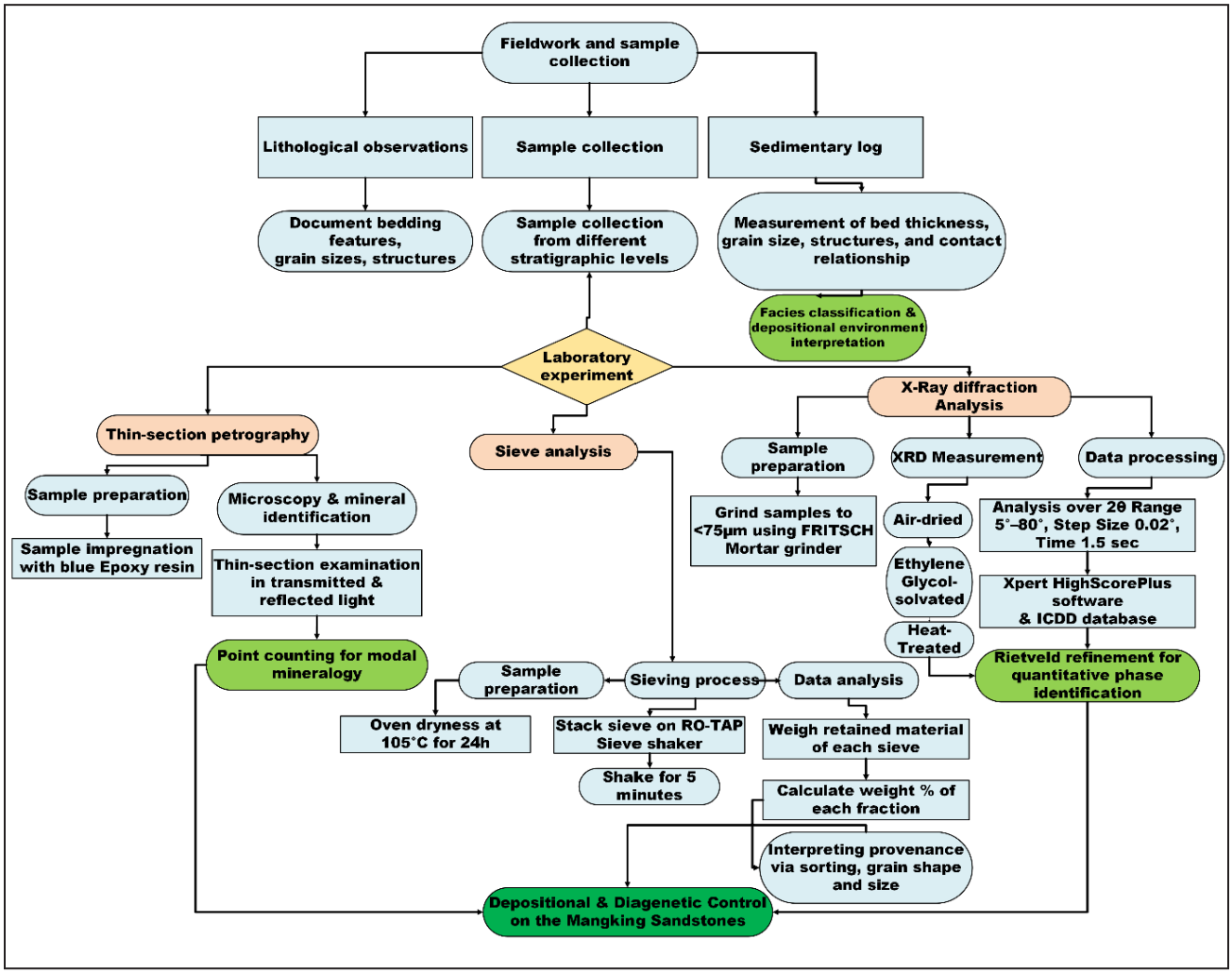


Figure 2: Methodological workflow.

METHODOLOGY

This work employed a multi-disciplinary approach integrating fieldwork and laboratory analyses (Figure 2) to evaluate the sedimentological and diagenetic controls on the reservoir quality of the red beds of Mangking Sandstones. Ten (10) samples were collected for this study due to restricted outcrop accessibility and dense tropical vegetation along Tembeling River and Kuala Tahan to Kampung Bantal road. Most accessible outcrops were confined to roadcuts and riverbanks, as thick forest cover and intense weathering in the humid Malaysian climate limit exposure of fresh, continuous sections.

Fieldwork, sedimentary facies and sample collection

Through detailed fieldwork, a sedimentological study was carried out at some selected outcrops of the red beds in the Mangking Sandstones. Field observations focused on lithological variations, facies characteristics, sedimentary structures and stratigraphic relationships (Figure 2). Emphasising freshness, representative samples were collected from different stratigraphic levels to ensure a detailed and comprehensive analysis of the diagenetic controls and processes responsible for the deposition of the sediments. Field outcrop photographs were taken to document bedding features, grain size variations, and sedimentary structures.

A sedimentary log was constructed based displaying observed sections along Tembeling River and Kuala Tahan to Kampung Bantal road (Figure 3). Bedding orientations at different stratigraphic sections were measured using a Brunton compass. Different lithofacies were identified based on descriptions of rock texture, mineral composition, colour, and sedimentary structures, with the classification scheme of Miall's (1985) also adopted in the facies description. These were further classified based on standard facies models, which allow the interpretation of depositional environments. In total, nine (9) outcrops were examined across the study area, and all were logged in detail for sedimentological and diagenetic characteristics.

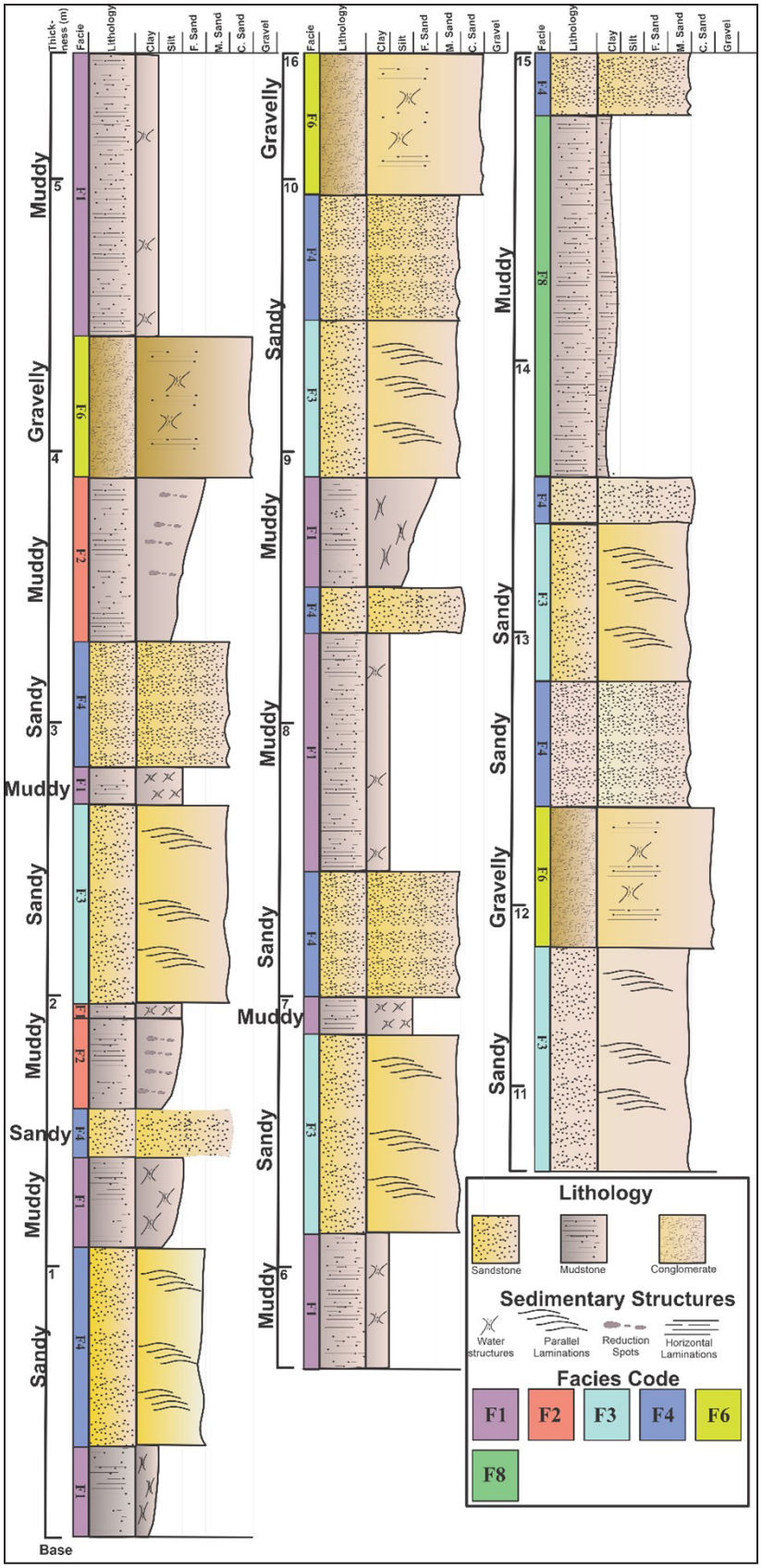


Figure 3: Sedimentary log sections of the Mangking Sandstone along Tembeling River and Kuala Tahan to Kampung Bantal road.

Thin-section analysis

Petrographic analysis was conducted on ten rock samples following standard laboratory procedures by Reed & Mergner (1953) and Bello *et al*. (2021) at the Geoscience Teaching Lab 3, Centralised Analytical Laboratory (CAL), Universiti Teknologi Petronas. All samples were impregnated with a blue-dyed epoxy resin before thin sectioning to enhance pore visibility. This procedure involved mixing 100 g of epoxy resin with 23 g of hardener (85 ml/20 ml ratio), followed by continuous stirring for at least three minutes. Each sample was then positioned at the centre of a mounting cup, and the epoxy mixture was carefully poured to ensure complete coverage.

The impregnated samples were placed inside a VACUMET 52 vacuum chamber, with the vacuum initially set to 560 mmHg. Air bubbles were observed within the mounting mixture and were allowed to dissipate for approximately 45 minutes. To further enhance resin penetration into pore spaces, the vacuum was adjusted to 100–130 mmHg, and the samples were left to cure for eight hours to ensure complete hardening.

The prepared thin sections were examined under a polarising optical microscope in both transmitted and reflected light to identify porosity, microfractures, mineralogical composition, textural relationships, and diagenetic features. The discrimination of quartz, hematite, and other clay minerals was conducted through both plane- and cross-polarised light microscopy. In addition, point counting was performed using JMICRONS software by counting 250 points per thin section to quantify the modal mineralogy and porosity of the samples.

X-ray diffraction (XRD) analysis

The mineralogical composition of the sandstone samples was determined using an X-ray diffraction (XRD) analysis conducted at the Centralised Analytical Laboratory (CAL), Universiti Teknologi Petronas. To ensure homogeneity, all samples were ground to a very fine powder (<75 μm) using FRITSCH Mortar Grinder and were then mounted

on sample holders and analysed over a 2θ range of 5° to 80°, with a step size of 0.02° and a counting time of 1.5 seconds per step.

Data processing and phase identification were performed using the Xpert HighScorePlus software, which employs both the International Centre for Diffraction Data (ICDD) Powder Diffraction File (PDF) database and the Crystallography Open Database (COD) (Amao *et al*., 2016). Quantitative phase analysis was carried out using the Rietveld refinement method implemented in the Xpert HighScorePlus software to determine the relative proportions of each mineral phase. The XRD results provided insights into the mineralogical composition of the sandstone samples, which aids in the interpretation of sedimentological and diagenetic processes that affect reservoir quality.

For clay mineral identification, oriented clay fraction mounts (<2 μm) were prepared following standard procedures by Dorothy (1970). The clay-sized fraction was separated by sedimentation and analysed under heat-treated, ethylene glycol-solvated, and air-dried conditions. Heat treatments were performed at 300°C and 550°C to assess the thermal stability of clay minerals and to differentiate illite, chlorite and kaolinite based on changes in basal reflections. Glycolation was carried out by exposing the samples to ethylene glycol vapour at 60°C for 24 hours to distinguish expandable clay minerals such as smectite and mixed-layer illite–smectite. Clay mineral identification was achieved by comparing peak positions and intensity variations across the different treatments, following established XRD diagnostic criteria.

Grain size analysis for sandstone

Following standard procedures described by Robertson *et al*. (1984), sieve analysis was conducted using a RO-TAP sieve shaker at the Teaching Lab 2, Civil Engineering Department, Centralised Analytical Laboratory (CAL), Universiti Teknologi Petronas, to determine the grain size distribution.

The samples were first air-dried to remove moisture content, which was then disaggregated using a mortar and pestle to break down any cemented particles while ensuring minimal alteration to grain morphology. According to ASTM D422 standards, approximately 100 grams of each sample were weighed and placed in a stack of sieves arranged in descending order of mesh size, ranging from 2 mm (coarse sand) to 63 μm (silt-clay boundary).

The sieve stack was secured onto the RO-TAP sieve shaker and subjected to mechanical agitation for 10 minutes to ensure effective separation of grain sizes. The vibration and tapping mechanisms facilitated the movement of particles through the sieves, allowing finer grains to pass through while retaining coarser particles in their respective sieves.

After sieving, the retained material on each sieve was carefully collected and weighed using a precision balance. The weight percentage of each fraction was calculated relative to the total sample weight. A grain size distribution curve was plotted using a semi-logarithmic scale, with particle size on the x-axis and cumulative percentage passing on the y-axis.

RESULTS

Sedimentary facies

Field observations across accessible and well-exposed sections of the Mangking Sandstones (Figure 3) led to the identification of six distinct lithofacies. These include; Mudstone with thin sandstone stripes (F1) (Figure 4B), Silt/mudstone (F2) (Figure 4C), Fine- to medium-grained laminated sandstones exhibiting soft sediment deformation structure (F3) (Figure 4D), Fine- to medium-grained sandstone (F4) (Figure 4E), Clast-supported conglomerate

Table 1: Summary of facies characteristics of the red beds in the Mangking Sandstones, Tembeling Group, including lithology, colour, thickness, and sedimentary features.

Facies codes	Lithology	Colour	Description
F1	Mudstone with thin sandstone stripes	Grey to brown	1 to 1.5m thick; massive and tilted; high proportion of clay minerals; thin laminations of grey mud/claystones.
F2	Silt(dud)stones	Light grey to brown	1 to 1.5m thick mudstone; reduction spot, mud spots, weathers into small to medium fragments.
F3	Fine- to medium-grained laminated sandstones	White to brown	0.3 m thick; parallel lamination resembling soft-sediment; poorly to medium sorted; medium rounded; medium proportion of clay and silt.
F4	Fine- to medium-grained sandstone	Grey to brown	0.3 to 0.5m thick; massive; poorly sorted; angular to medium rounded.
F6	Clast-supported conglomerate	White to light grey	0.2 to 0.4m thick; well-defined clay laminations; poorly sorted.
F8	Mudstones	Red to brown	>5m thick; massive, non-laminated.



Figure 4: Outcrop photographs showing the sedimentary sections and the assigned lithofacies within the Mangking Sandstones, Tembeling Group. (A) Mudstone with thin sandstone stripes (F1). (B) Silt/mudstone with reduction spot (F2). (C) Fine- to medium grained laminated sandstones exhibiting soft sediment deformation structure (F3). (D) Fine- to medium-grained sandstone (F4). (E) Clast-supported conglomerate (F6). (F) Massive, non-laminated mudstones (F8).

(F6) (Figure 4G) and Massive, non-laminated mudstones (F8) (Figure 4I) were identified, each representing different depositional events and diagenetic histories (Table 1).

Facies association

The six (6) facies identified in the Mangking Sandstones were interpreted based on their sedimentological characteristics and stratigraphic relationships. To better understand the depositional settings, these facies were grouped into three major facies associations: Gravelly Facies association, Sandy Facies association, and Muddy Facies association. Each association reflects distinct depositional processes and environmental conditions of the Mangking Sandstones. The sedimentary log shown in Figure 3 provides a detailed visual representation of these facies and their vertical arrangement within the Mangking Sandstone along the Tembeling River and Kuala Tahan to Kampung Bantal road.

Muddy Facies association

Description:

The Muddy Facies in this work includes F1 (Mudstone with thin sandstone stripes), F2 (Mudstones), and F8 (Mudstones/siltstones), especially in the lower parts of the studied sections (Figure 3). Facies F1 is composed of grey to brown and massive mudstones with predominant water structures and thin laminations of claystones or sandstones (Figure 3; Figure 4B). Facies F2 consists of light grey to brown, massive mudstones with reduction spots (Figure 3; Figure 4C). Facies F8 presents as thick, massive red to brown mudstones. The sedimentary log (Figure 3) shows the prominent presence of Muddy Facies, particularly in the lower portions of the studied section. Facies F1 is the oldest, deposited at the base. Facies F2, a mudstone, is separated from facies F1 by a thin layer of sandstones. Facies F8, represented by mudstones/siltstones, is mostly massive with no observable structures and range in thickness from 7 meters to over 8 meters.

Interpretations:

Collectively, muddy facies association point to distal fluvial settings characterised by low energy, episodic flooding, and periods of landscape stability conducive to soil development (Batezelli *et al*., 2019; Collins *et al*., 2020). Facies F1's high clay content and lack of sorting suggest suspension settling typically interpreted as overbank or drape deposits from waning floods. Facies F2's pedogenic features indicate periods of subaerial exposure and soil

development. Facies F8 is consistent with the Fl facies and likely formed from slow-settling fine sediments in overbank environments during flood events or in shallow standing water. The recurrent appearance of these muddy facies throughout the log indicates repeated episodes of overbank deposition and floodplain development.

The vertical sequence often shows transitions from muddy to sandy and then sometimes to gravelly units, followed by a return to muddy or sandy units, reflects fluctuating fluvial dynamics from low-energy floodplains to higher-energy channel environments.

Sandy Facies association

Description:

The Sandy Facies association were deposited in the middle to upper parts of the studied sections and comprises F3 (Fine-to-medium-grained laminated sandstones) and F4 (Fine-to-medium-grained sandstones) (Table 1). Facies F3 is made up of thin, horizontally laminated sandstones that are moderately sorted and contain a variable amount of silt and clay. Facies F4 consists of red to brown, massive, and poorly sorted coarse sandstones, with angular to medium-rounded clasts and rip-up clasts up to 15 cm in size (Table 1).

Interpretations:

The sedimentary features of Facies F3 are consistent with Miall's (1985) Sh facies, indicating deposition from planar bed flows under lower flow regime conditions, likely in channel bar tops or sheet flow environments. Facies F5 fits the St code of Miall's (1985) classification, representing planar cross-bedded sands deposited by migrating bars or sand waves under variable flow regimes. Facies F7, also assigned to Sh, suggests similar depositional processes. These sandy facies are suggested to interpret as deposits from active channel systems, including bar migration zones and channel margins, where sediment transport and deposition occurred under fluctuating but generally moderate flow conditions (Glad *et al*., 2019). These facies also exhibit characteristics consistent with the channel bar complex identified by Azmi *et al*. (2020). The interbedding of these sandy facies with the muddy facies observed in the sedimentary log highlights dynamic shifts in channel activity and sediment supply within the depositional environment.

Gravelly Facies

Description:

The Gravelly Facies was found in the upper sections of most outcrops and includes F4 (Coarse-grained sandstones to fine-grained conglomerates) and F6 (Clast-supported conglomerate). Facies F6 is composed of white to light grey, poorly sorted, clast-supported conglomerates with clay laminations. These facies show a fining-upward sequence capped by thin mudstone (Figure 3).

Interpretations:

These gravelly facies are interpreted as representing proximal, energetic fluvial settings where sediment was rapidly deposited with minimal reworking. Facies F6, with its clast-supported fabric and lenticular geometry, suggests deposition from grain-dominated flows confined within channelised environments. Similar to clast-supported conglomerate interpreted by Chung *et al*. (2023), it likely represents gravel sheet deposits or low-relief longitudinal bars formed under high-velocity flood conditions. According to Miall's (1985) classification, F4 corresponds to the Gm facies (massive or crudely bedded gravels) commonly deposited under intense flow conditions in braided rivers or proximal alluvial fan environments. The vertical transition from muddy Facies to coarser sandstones or conglomerates observed in the sedimentary log (Figure 3) may represent a progradational trend, indicating increasing flow energy over time within the fluvial system.

Petrographic analysis

Detrital and authigenic composition

The modal composition of selected samples from the Mangking Sandstones reveals a diverse assemblage of grain-contact types, cements and detrital grains. Among the detrital components, quartz (Q) is the most dominant constituent, with values ranging from 17.7% to 32.7%, and an average of 26.5% (Figure 5H; Table 1). Matrix content (MX) is another major component, with values between 11.3% and 18.0%, and an average of 14.6% (Table 2). Illite (I) is the predominant clay type found in most of the samples (avg. 3.6%) (Figure 5J). It appears yellowish to dark brown under thin sections and is mostly found in association with hematite. While illite-smectite (IS) appears in virtually all samples (4.0 - 11.3%, avg. 7.1%) (Table 2), it is observed in various samples in the form of grain-coating around quartz grains. Kaolinite is absent in most samples and was not identified from thin section photomicrographs. Its presence is detected by XRD analysis in two samples (avg. 0.4%) (Table 2). Muscovite was detected in small proportions (0.7% - 3.3%, avg. 1.9%) (Figure 5B). Its presence, according to Kamp & James (2022), posits a metamorphic origin in terms of sediment provenance.

In terms of grain contacts, point contact (PC) and long contact (LC) were observed in relatively low abundances (avg. 1.8% and 1.5%) (Figure 5F). Among the diagenetic features, quartz overgrowth (QO) occurs in preponderance relative to other cements (averaging 16.2%) (Figure 5A). Based on the thin section observation, it exhibits various morphologies at the edges of quartz grains. In addition, it is coated by hematite and smectite along grain contacts (Figure 5K). Hematite and magnetite constitute minor authigenic cements within the studied samples (Table 2). These cements exhibit dark brown to black colour and mostly occur both as grain-coating and pore-filling in various thin section photomicrographs (Figure 5C, L), resulting in a

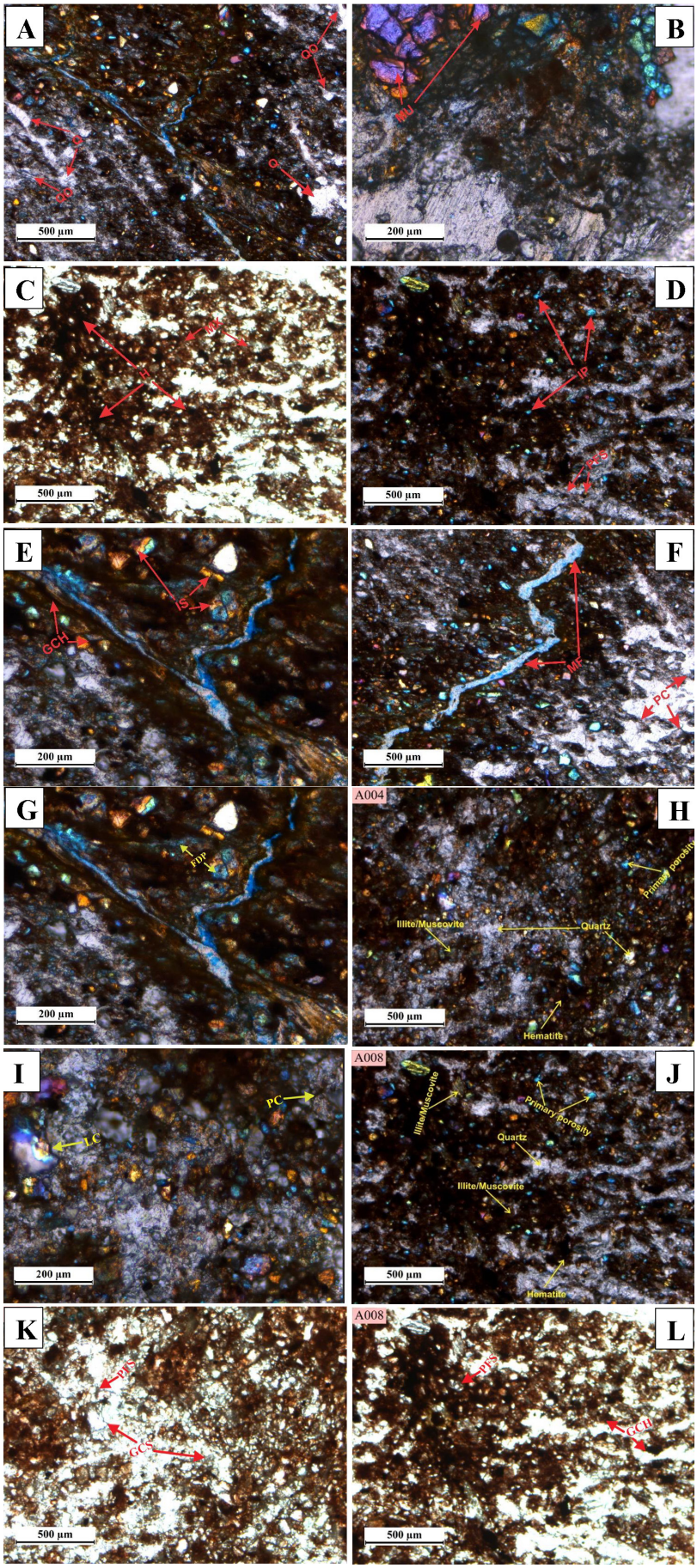


Figure 5: Photomicrographs (cross and plain polarized light) of the main type of framework grains within the studied samples. (A) Q = quartz, QO = quartz overgrowth (XPL). (B) MU = muscovite. (C) H = hematite (PPL). (D) IP =Intergranular porosity. (E) IS = illite-smectite, GCH = grain-coating hematite. (F) MF = micro-fracture (XPL). (G) FDP = Feldspar dissolved porosity (XPL). (I) LC = Long contact, PC = Point contact MX = matrix; MG = magnetite; K = kaolinite; LC = long contact; PC = point contact (XPL). (K) PFS = pore-filling smectite; GCS = grain-coating smectite (PPL). (L) GCH = Grain-coating hematite (PPL)].

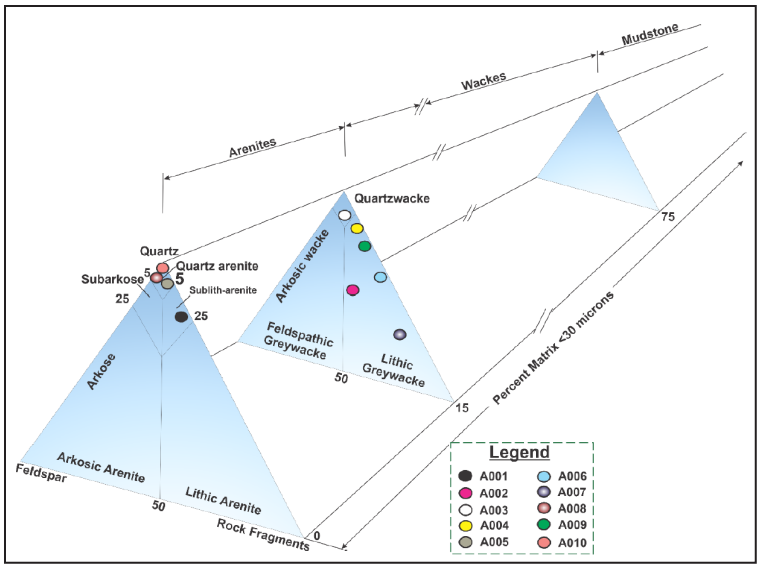


Figure 6: Classification of terrigenous sandstones based on quartz, feldspar, and rock fragments – a Ternary Plot representing the modal composition of the red beds in Mangking Sandstone, Tembeling Group (modified from Pettijohn *et al*., 1974).

loss in intergranular porosity. Feldspar cement has not been observed in any sample, which could have possibly dissolved due to the climatic conditions of the region. Pore-filling smectite (PFS) (Figure 5K) and grain-coating smectite (GCS) (Figure 5L) were observed in small percentages in some samples, which further contribute to porosity reduction. In terms of porosity indicators, intergranular/primary porosity (IP) ranges from 3.7% to 9.3%, averaging 6.0% (Table 2), while micro-fractures (MF) are less common (Figure 5E, F) and completely absent in some samples.

According to Pettijohn *et al*. (1974), classification of terrigenous sandstones based on quartz, feldspar, and lithic fragments majority of the samples fall under lithic greywacke then followed by quartz arenites with quartzwacke in lesser amount whereas a little or complete absence of feldspathic greywackes and arkosic arenite has been observed (Figure 6).

Grain sorting and provenance

Each sieve sample was assigned to a facies association (Muddy, Sandy or Gravelly) using the grain-size distributions from the sieve analysis conducted in the laboratory. The sandy facies include A001, A002, A003, A006, A007 and A010 (corresponding to F3 and F4 depending on coarseness and structure) while A004 and A005 belong to gravelly facies (F6) and A008 represents a typical muddy facies (F1/F2/F8). These allocations are based on the relative weight retained in the coarse sieves, in the pan, and the median grain size derived from the cumulative distributions.

Sorting, which refers to the uniformity of grain sizes within a sample, varies among the analysed samples. From the shape of the grain size distribution curves (Figure 7), it can be inferred that nearly all the samples appeared to be uniformly graded, which indicates a relative homogeneity in the grain sizes. The sandy facies show median diameters in the fine–to–coarse sand range, exhibiting medium to poor sorting in several samples. Sample A005 is dominated by

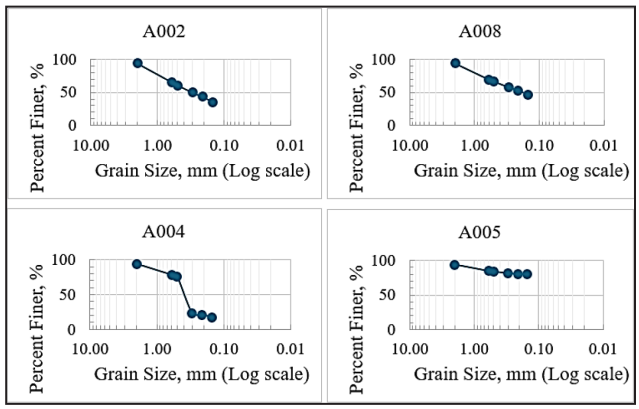


Figure 7: Grain size distribution curves for some selected samples.

very coarse fractions and shows extreme poor sorting. This posits a clear signal of gravelly, proximal deposition (F6). The grain-size signature (> coarse sieves) is consistent with grain-supported conglomerates.

The lithic ternary plot further refines the source characterisation by categorising the lithic fragments into metamorphic (Lm), volcanic (Lv), and sedimentary (Ls) components (Figure 8). The clustering of data points towards the Ls and Lm fields suggests a provenance dominated by recycled sedimentary rocks and low-grade metamorphic sources. This points to a depositional setting influenced by uplifted orogenic belts, where pre-existing sedimentary sequences were eroded and reworked. In addition, this is supported by Krynine's (1948) first proposed idea, which suggested that the continental crust is made up of sedimentary layers producing quartz-rich quartzite, metamorphic rocks generating lithic-rich greywacke, and deeper plutonic rocks creating feldspar-rich arkose.

Bulk mineralogical analysis

The XRD-based quantitative mineralogical analysis of the Mangking Sandstones reveals a framework predominantly

Table 2: Summary of petrographic point count data and whole-rock XRD bulk mineralogy for sandstone samples.

Detrital Grains (%)									Cement and Grain contacts (%)							
Sample ID	Q	I	IS	H	MU	MX	MG	LC	PC	FG	PFS	GCS	QO	GCH	IP	MF
A001	17.7	5.3	11.3	10.3	3.3	11.3	0.0	1.0	1.7	0.0	2.7	2.3	18.3	6.0	5.7	3.0
A002	20.7	5.3	4.0	9.7	2.3	11.3	1.3	2.3	3.0	0.0	4.3	4.0	16.7	7.0	5.7	2.3
A003	30.0	4.7	7.0	6.0	1.3	14.3	0.0	1.7	2.3	0.0	3.3	2.7	16.3	6.7	5.7	1.3
A004	23.0	3.3	7.3	8.0	0.7	18.0	0.0	2.3	0.7	0.0	2.0	3.7	15.0	9.0	7.0	0.0
A005	32.3	2.0	6.7	4.0	1.0	15.7	0.0	1.0	1.3	0.0	2.0	2.0	18.0	5.7	6.0	1.0
A006	25.7	3.3	6.0	7.7	2.7	16.0	0.3	1.3	2.0	0.0	3.7	3.3	15.3	6.3	5.3	1.7
A007	23.0	5.0	8.0	8.3	2.7	14.0	0.7	2.0	2.7	0.0	4.0	4.0	14.7	8.0	6.3	1.0
A008	32.7	3.3	7.3	6.7	1.0	18.0	0.0	1.7	2.3	0.0	1.0	5.0	11.7	5.7	3.7	0.0
A009	28.7	1.7	6.0	5.3	2.0	13.3	0.0	1.0	1.7	0.0	2.3	2.3	17.3	6.7	5.3	0.7
A010	31.3	1.7	7.3	2.3	2.3	14.3	0.0	0.7	0.7	0.0	3.3	1.0	18.3	7.3	9.3	0.0
Min	17.7	1.7	4.0	2.3	0.7	11.3	0.0	0.7	0.7	0.0	1.0	1.0	11.7	5.7	3.7	0.0
Max	32.7	5.3	11.3	10.3	3.3	18.0	1.3	2.3	3.0	0.0	4.3	5.0	18.3	9.0	9.3	3.0
Average	26.5	3.6	7.1	6.8	1.9	14.6	0.2	1.5	1.8	0.0	2.9	3.0	16.2	6.8	6.0	1.1

Results of the whole-rock XRD analysis (Bulk mineralogy in wt. %)							
Sample ID	Q	I	IS	H	MU	MG	K
A001	78.1	11.7	19.4	0.4	9.9	0.0	0.0
A002	54.0	0.0	0.0	1.9	24.3	0.5	0.0
A003	91.1	6.7	0.0	0.0	0.0	0.0	2.2
A004	74.6	0.0	0.0	1.6	23.8	0.0	0.0
A005	100	0.0	0.0	0.0	0.0	0.0	0.0
A006	69.4	6.0	0.0	0.0	24.6	0.0	0.0
A007	60.4	15.0	0.0	9.8	14.7	0.0	0.0
A008	66.6	11.4	0.0	3.0	19.0	0.0	0.0
A009	100	0.0	0.0	0.0	0.0	0.0	0.0
A010	90.9	7.1	0.0	0.0	0.0	0.0	2.0
Min	54.0	0.0	0.0	0.0	0.0	0.0	0.0
Max	100	15.0	19.4	9.8	24.6	0.5	2.2
Average	78.51	5.79	1.94	1.67	11.63	0.05	0.42

[Q = quartz; I = illite; IS = illite-smectite; H = hematite; MU =muscovite; MX = matrix; MG = magnetite; K = kaolinite; LC = long contact; PC = point contact; PFS = pore-filling smectite; GCS = grain-coating smectite; QO = quartz overgrowth; GCH = grain-coating hematite; IP =Intergranular porosity; MF = micro-fracture]

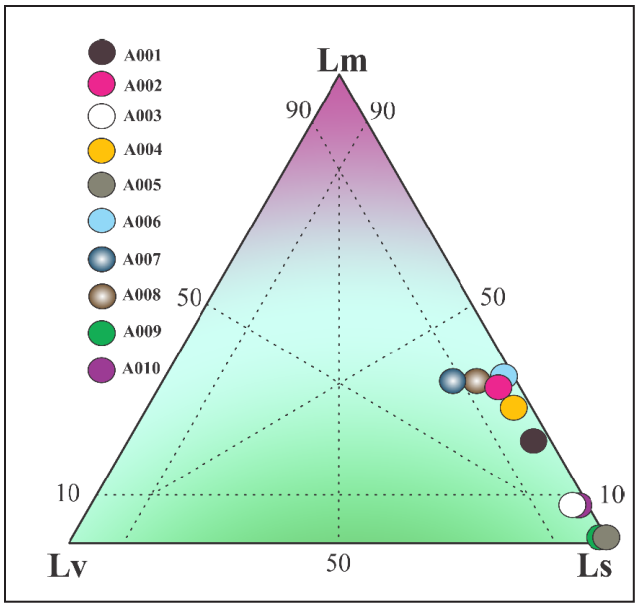


Figure 8: Lithic composition of sandstones based on provenance types – A Ternary Plot showing the distribution of lithic metamorphic (Lm), lithic volcanic (Lv), and lithic sedimentary (Ls) components (modified from Garzanti, 2019).

composed of quartz, with values ranging from 54.0% to 100.0% (avg. 78.51%) and a high average concentration across all samples (Table 2). Muscovite is the second most abundant mineral phase, with concentrations reaching up to 24.6% and a consistent presence in most samples (Table 2). Common clay mineral, particularly illite, including its mixed-layer variant illite-smectite, was also observed (avg. 5.79%). Kaolinite was detected in minor amounts (ranges from 0.0% to 2.2%) (Table 2). On the other hand, hematite (the highest content recorded in some samples up to 9.8%) and magnetite occur in trace to minor amounts.

Grain dissolution and secondary porosity

Thin-section examination of the studied samples revealed the development of secondary porosity likely due to the dissolution of feldspar grains within the sandstones. These porosities are identified as irregular (Figure 5G), selectively etched voids where feldspar grains have undergone near-complete dissolution, likely due to post-depositional geochemical alteration under acidic pore fluids.

DISCUSSION

Effects of diagenesis on the Mangking Sandstones

Diagenesis results in a lasting imprint on the textural, compositional, and pore characteristics of sandstones. This is generally considered as a key to determining whether a formation becomes a viable reservoir or remains a tightly cemented rock mass. In this study, petrographic observations of the Mangking Sandstones revealed a complex interplay of compaction, cementation, mineral alteration, and

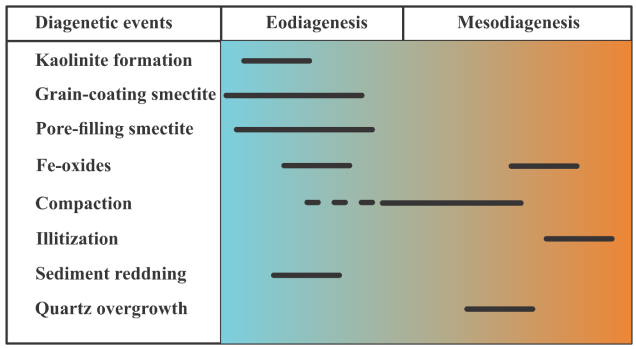


Figure 9: Diagenetic processes influencing the continental red beds of the Mangking Sandstones, illustrating the timing of key diagenetic events during eodiagenesis and mesodiagenesis.

dissolution, which has significantly reshaped the original sediment fabric, influencing both reservoir quality and post-depositional history. These petrographic observations, based on identified diagenetic minerals, indicated that the Mangking Sandstones underwent both shallow diagenesis (eodiagenesis, <2 km/<70°C) and relatively deep-burial (mesodiagenesis, >2 km/>70°C) (Figure 9).

The early diagenetic impression in the Mangking Sandstones is evidenced by a suite of authigenic minerals and microstructural features that reflect shallow burial, oxidising conditions, and early fluid-rock interactions. Early diagenesis (i.e., eodiagenesis) is characterised by processes that occur at shallow depths under low temperatures where meteoric or marine pore waters dominate and sediment is still loosely compacted (Morad *et al*., 2000; 2010). One of the most diagnostic early diagenetic features in the Mangking Sandstones is the presence of grain-coating hematite (Figure 5K). These coatings are typical products of early subaerial exposure or well-oxygenated vadose environments, as described by Bello *et al*. (2023), and suggest that the Mangking Sandstones were deposited under oxidising continental conditions. The grain-coating hematite likely formed before significant compaction, preserving grain outlines and inhibiting quartz overgrowth, which is a well-documented early diagenetic control on porosity evolution. The occurrence of both pore-filling smectite and grain-coating smectite further underscores early diagenetic processes because smectite is known to form in low-temperature environments from the alteration of volcanic ash or unstable feldspars and can infiltrate as detrital or pedogenic clays in fluvial settings (Wilson, 1992; McKinley *et al*., 1999). Consequently, the presence of smectitic phases at shallow depths tends to reduce permeability by occluding pore throats, however, they can also delay quartz cementation by shielding grain surfaces. Kaolinite (although detected in a few samples) and grain-coating smectite are believed to have formed during early diagenesis under shallow burial conditions at temperatures below 70°C (Worden & Burley, 2003; Morad *et al*., 2000; 2010). Mechanical compaction began during this early diagenetic stage, following the development of grain-coating clays (Figure 9).

Evidence from the Mangking Sandstones reveals several features consistent with mesodiagenetic processes, as outlined by Morad *et al*. (2000). One of the most prominent indicators is the occurrence of quartz overgrowths (Figure 9), which has been observed in all the samples within the Mangking Sandstones (Table 2). These authigenic overgrowths result from pressure solution and the subsequent re-precipitation of silica at grain contacts. This process is typically activated at burial depths exceeding 2–3 km and temperatures above 60–70°C. Such transformation reduces intergranular porosity and reflects prolonged exposure to silica-saturated fluids during deep burial.

The consistent presence of illite across all the samples, alongside the complete absence of feldspar and only trace concentrations of kaolinite (Table 2), suggests that the formation has undergone adequate burial and thermal exposure to facilitate the complete conversion of feldspar and much of the kaolinite to illite. Such a mineralogical assemblage reflects a more advanced stage of burial diagenesis compared to formations like the Gombe Sandstone (Bello *et al*., 2023), where co-existing kaolinite and K-feldspar indicate limited thermal exposure and incomplete illitization. Therefore, the observed mineralogy in the Mangking Sandstones is interpreted to result from progressive burial diagenesis under conditions that promoted the near-complete transformation of reactive silicate phases into illite, indicative of a relatively mature diagenetic environment.

Another important burial signature is the presence of feldspar dissolution porosity (Figure 5G), based on the intergranular porosity (IP) spotted in various samples (Figure 5D). Previous works (Morad *et al*., 2000; Worden & Burley, 2003; Morad *et al*., 2010) deduced that feldspar dissolution is commonly driven by organic acid generation during hydrocarbon maturation or the influx of CO_2-rich formation waters, leading to secondary porosity enhancement. The presence of microfractures may also be attributed to burial-related tectonic stress or overpressure development, providing additional pathways for diagenetic fluid migration and enhancing late-stage cementation or dissolution.

The impact of different facies on reservoir quality

Compaction

Deep burial coupled with effective stress exerts morphological changes to sediments. As the depth of burial increases, mechanical compaction results in grain rotation, repacking and rearrangement, grain fracturing, and ductile deformation of soft grains (Bello *et al*., 2024). Facies analysis and petrographic observations of grain-to-grain contacts documented in this study provided insights into how diagenesis is linked to depositional facies within the Mangking Sandstones. Samples obtained from the muddy facies association display the highest proportions of long grain-to-grain contacts (2.3% and 1.7%, Table 2). This is interpreted to have likely experienced an advanced mechanical compaction in their fine-grained, clay-rich matrices. Such fabrics suggest early pore throat closure and significant loss of primary intergranular porosity during the initial burial stages. Additionally, this interpretation is corroborated by the complete absence of micro-fractures in the muddy facies (0.0%), compared to the sandy and gravelly depositional facies (Table 2)

In contrast, samples from sandy facies association exhibit intermediate long-contact values (1.0% and 2.3%), reflecting moderate mechanical compaction consistent with their coarser grain size and lower matrix content. The persistence of point contacts within these units implies that a portion of the original porosity has been retained. Gravelly facies, characterised by the lowest incidence of long grain-to-grain contacts (0.7%), demonstrates minimal mechanical compaction. This is attributed to the dominance of coarse, rigid clasts that resist compactive deformation. Such characteristics support the interpretation by Bello *et al*. (2023) that during progressive burial, gravelly facies tend to preserve higher primary intergranular porosity compared to finer-grained counterparts. These trends align with experimental observations that mechanical compaction is more pronounced in fine-grained, clay-rich deposits due to their higher initial packing density and the ductile behaviour of the matrix.

Cementation

Cementation during diagenesis exerts a critical control on reservoir quality by occluding pore spaces and reducing permeability, with both early (eodiagenetic) and late (mesodiagenetic) phases playing distinct roles. The muddy facies, for instance, exhibits high concentrations of grain-coating smectite (up to 5.0%) and pore-filling smectitic clays ranging from 1.0–2.0%. These clays, derived largely from the alteration of feldspathic or volcanic grains and redistributed by meteoric waters during shallow burial (<70 °C), significantly reduce intergranular porosity (down to 3.7%), effectively choking pore throats and impeding permeability at an early stage (Worden & Burley, 2003; Morad *et al*., 2010).

In contrast, the sandy facies reveals a broader spread in both grain-coating smectite and pore-filling clay cements, with notable samples such as A002 and A007 showing elevated levels of both GCS (4.0%) and PFS (4.3%). These concentrations correspond to moderately low porosity values (5.7–6.3%), indicating intermittent influxes of detrital clays or early diagenetic precipitation that locally impair fluid connectivity despite cleaner grain frameworks (Figure 10a).

During mesodiagenesis, quartz cementation becomes the dominant porosity-reducing process, particularly in coarser-grained deposits. Gravelly facies association exhibits the highest abundance of quartz overgrowths (18.3%), and also retains the highest intergranular porosity (9.3%). This paradox may reflect incomplete quartz cementation at grain contacts due to grain coating inhibition or limited burial

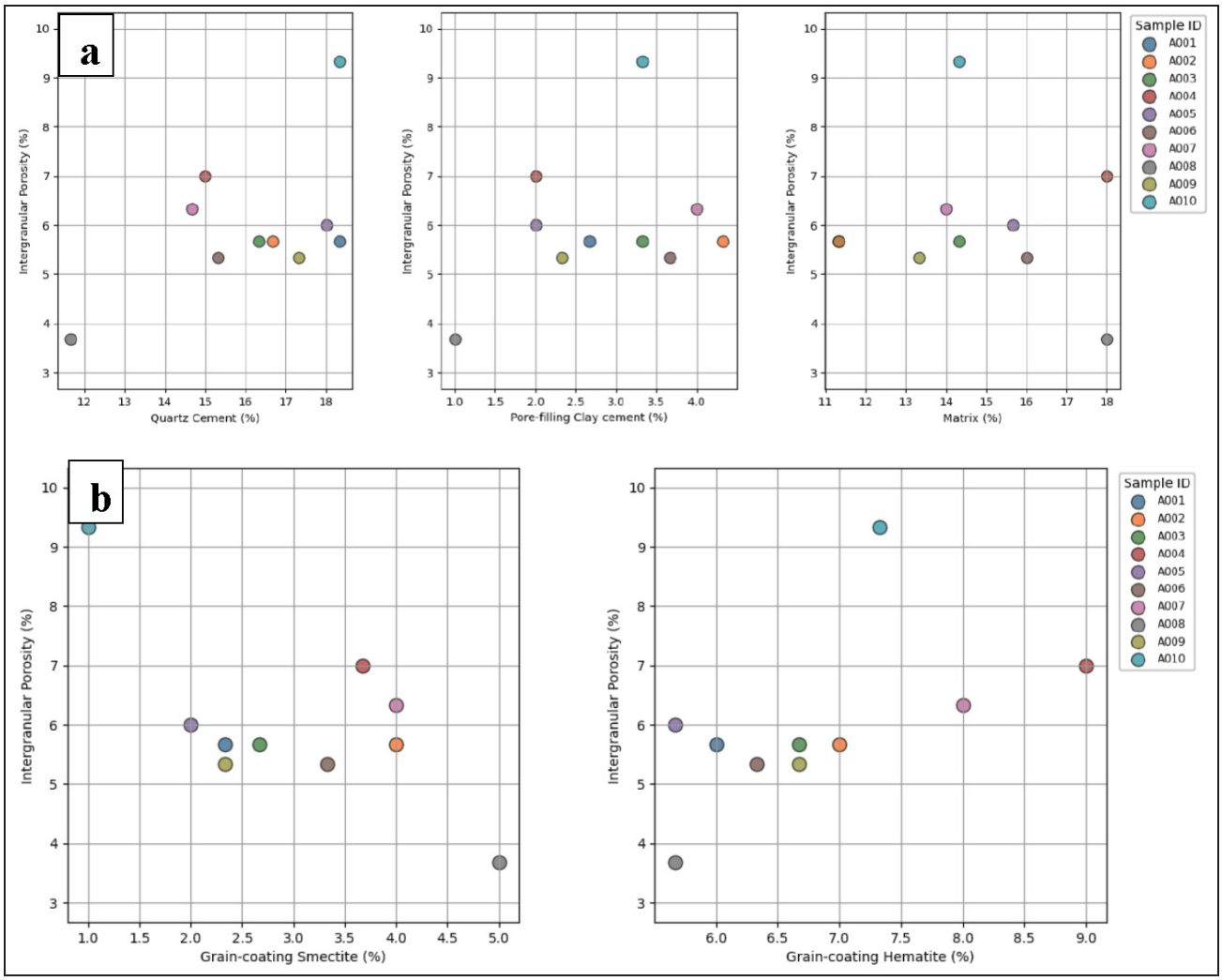


Figure 10: Crossplots of intergranular porosity versus diagenetic components.
(a) Intergranular porosity versus quartz cement, pore-filling clay cement, and matrix content.
(b) Intergranular porosity versus grain-coating and pore-filling clay cements, showing an inverse relationship between clay cementation and porosity, with smectite- and hematite-rich samples exhibiting lower porosity.

duration, despite a silica-saturated environment (>70 °C) conducive to cementation (Cook *et al*., 2011; Busch *et al*., 2024). By contrast, muddy and sandy samples show significantly reduced porosities, suggesting a combined effect of matrix and early clay cement occlusion along with quartz overgrowths (Figure 10a).

The effect of iron oxide cementation is also observed in the form of hematite grain coatings, most prominent in samples such as A004 and A007 with concentrations ranging between 8.0–9.0% (Figure 10b). These coatings likely precipitated under oxidising, near-surface conditions and formed rigid films around grains that not only reduce effective pore throat sizes but may also inhibit subsequent quartz cementation (Morad *et al*., 2010; Worden & Burley, 2003). Notably, samples with higher hematite content still maintain moderately high porosity (~7.0%), which suggests that in some cases hematite coatings may preserve primary porosity by delaying mechanical compaction and quartz cementation (Heald & Larese, 1974; Bello *et al*., 2024).

In general, the variation in cement types and their spatial distribution across facies controls the observed spread in intergranular porosity, demonstrating the complex interplay between early diagenetic input, burial depth, and fluid composition during reservoir evolution.

CONCLUSION

The Mangking Sandstones were deposited in a fluvial-dominated system (with both channel and overbank deposits) consisting of mudstone, fine and medium-grained sandstone and conglomerates that are uniformly graded with a preponderance of lithic greywacke owing to the high matrix content.

Given the lowest occurrence of long grain-to-grain contacts (0.7%) and low matrix content (14.6%), gravelly facies are considered to have the best reservoir quality in

comparison to the muddy facies, which are characterised by a high proportion of long grain-to-grain contacts (2.3%). In contrast, the sandy facies exhibits intermediate reservoir quality, attributed to moderate mechanical compaction and the presence of coarser grains with lower matrix content, which suggests partial preservation of original porosity.

The Mangking Sandstones generally exhibit poor porosity, primarily limited to intergranular porosity (6.0%), which indicates that an insignificant portion of primary porosity has been preserved. However, additional contribution from micro-fractures (avg. 1.1%), although not available in all samples, enhances overall porosity and may improve permeability by providing secondary pathways for fluid flow.

Cementation (particularly quartz overgrowth) was the dominant process responsible for the significant reduction in intergranular porosity. The impact of cementation was compounded by the high matrix content across all samples (avg. 14.6%), with a more pronounced effect in the muddy facies compared to the gravelly and sandy facies.

The abundant presence of deep-burial cements, such as illite and quartz overgrowths, suggests that the studied Mangking Sandstone experienced prolonged residence in the mesogenetic realm. This is accompanied by significant evidence of early (eodiagenetic) processes, including kaolinite formation, grain-coating and pore-filling smectite, hematite coatings, and sediment reddening, indicating a complex diagenetic history involving both shallow and deep burial alterations.

The abundance of deep-burial cements, such as illite and quartz overgrowths, indicates that the Mangking Sandstone experienced significant burial and underwent prolonged residence in the mesogenetic realm. This was likely followed by tectonic uplift, which re-exposed the formation to near-surface conditions. As a result, early diagenetic (eodiagenesis) processes such as kaolinite formation, grain-coating and pore-filling smectite, hematite precipitation, and sediment reddening became prevalent.

Reservoir quality in the Mangking Sandstones is determined to be governed by the balance between depositional texture and diagenetic modification. Here, we conclude that facies deposited under higher-energy fluvial conditions retained better textural attributes for porosity preservation, yet subsequent diagenetic overprinting, particularly quartz and clay cementation, markedly reduced pore connectivity. Facies heterogeneity therefore translates into variable reservoir performance, where gravelly and coarse sandy units remain the most promising targets for fluid storage and flow. Integrating sedimentological and diagenetic insights provides a more predictive framework for assessing reservoir potential within the Upper Jurassic red beds of the Tembeling Group.

This study provides critical insights into the interplay between depositional processes and diagenetic alterations in controlling the reservoir quality of the Upper Jurassic red beds of the Mangking Sandstones. In addition to integrating sedimentological and petrographic data, the work establishes a predictive framework for identifying facies with better reservoir potential, particularly within fluvial-dominated systems. These findings are significant not only for advancing the understanding of red bed reservoir characteristics in Peninsular Malaysia but also for guiding future exploration and reservoir assessment strategies in similar continental settings worldwide.

ACKNOWLEDGEMENT

The authors thank the Petroleum Technology Development Fund (PTDF), Nigeria, for sponsoring the studies of Abdulrahman Muhammad. This research was conducted under the YUTP-FRG grant (Cost Centre 015LC0-489) from Universiti Teknologi PETRONAS, through the Institute of Hydrocarbon Recovery. The authors also thank the Centralised Analytical Laboratory (CAL), Universiti Teknologi PETRONAS, for access to the thin-section, XRD and grain-size analytical facilities. We are grateful to the anonymous reviewers and the editor for their constructive comments.

AUTHORS CONTRIBUTION

AM: Conceptualization, methodology, data curation, writing – original draft. **MSI:** Supervision, project administration, funding acquisition, validation, writing – review & editing. **HT:** Supervision, project, validation, writing – review & editing **AID:** Data collection, formal analysis, software. **AKS:** Visualisation, methodology, critical revision of manuscript.

CONFLICT OF INTEREST

The authors have no conflict of interest.

REFERENCES

Adepehin, E.J., Bankole, O.M., & Arifin, M.H., 2022. Poro-perm evolution in Oligo-Miocene coastal sandstones: Constraining the relative influence of sedimentary facies, mineralogy, and diagenesis on analogue reservoir quality of the Nyalau Formation, Borneo. Marine and Petroleum Geology, 139, 105589. https://doi.org/10.1016/j.marpetgeo.2022.105589.

Amao, A.O., Al-Ramadan, K., & Koeshidayatullah, A., 2016. Automated mineralogical methodology to study carbonate grain microstructure: an example from oncoids. Environmental Earth Sciences, 75(8), 666. https://doi.org/10.1007/s12665-016-5492-x.

Azmi, A.S.B., 2021. Sedimentology and Source Rock Evaluation of the Jurassic-Cretaceous Deposits in Central Phanag, Malaysia. Universiti Teknologi Petronas. (Doctoral dissertation) Universiti Teknologi Petronas, Perak.

Azmi, A.S., Ismail, M.S., Talib, J.A., & Samsudi, N.M., 2020. Environment of deposition of the Jurassic-Cretaceous continental deposit in central Pahang (Peninsular Malaysia) by sedimentary facies analysis. Bulletin of the Geological Society of Malaysia, 70, 153–162. https://doi.org/10.7186/bgsm70202013.

Bankole, O.M., El Albani, A., Meunier, A., Rouxel, O.J.,

Gauthier-Lafaye, F., & Bekker, A., 2016. Origin of red beds in the paleoproterozoic Franceville Basin, Gabon, and implications for sandstone-hosted uranium mineralization. American Journal of Science, 316(9), 839–872. https://doi.org/10.2475/09.2016.02.

Batezelli, A., Ladeira, F.S.B., Nascimento, D.L. do, & DA Silva, M.L., 2019. Facies and palaeosol analysis in a progradational distributive fluvial system from the Campanian–Maastrichtian Bauru Group, Brazil. Sedimentology, 66(2), 699–735. https://doi.org/10.1111/sed.12507.

Bello, A.M., Amao, A., Alqubalee, A., Al-Hashem, M., Albarri, H., Al-Masrahy, M., Al-Ramadan, K., & Babalola, L., 2024. Diagenetic Controls on Reservoir Porosity of Aeolian and Fluvial Deposits: A Case Study from Permo-Carboniferous Sandstones of Saudi Arabia. Arabian Journal for Science and Engineering, 49(1), 973–993. https://doi.org/10.1007/s13369-023-08590-2.

Bello, A.M., Jones, S., Gluyas, J., Acikalin, S., & Cartigny, M., 2021. Role played by clay content in controlling reservoir quality of submarine fan system, Forties Sandstone Member, Central Graben, North Sea. Marine and Petroleum Geology, 128, 105058. https://doi.org/10.1016/j.marpetgeo.2021.105058.

Bello, A.M., Usman, M.B., Amao, A.O., Salisu, A. M., Al-Ramadan, K., Abubakar, U., Mukkafa, S., Kwami, I. A., Chiroma, L.U., Al-Hashem, M., Yusuf, A., Maigari, A.S., Kachalla, A., Aro, O.E., Ismai'l, M. A., Umar, U.S., & Akinsanpe, O.T., 2025. Linking provenance and diagenesis to reservoir quality evolution of sandstones: The Paleocene-Eocene Kerri-Kerri Formation, northeastern Nigeria. Marine and Petroleum Geology, 172. https://doi.org/10.1016/j.marpetgeo.2024.107227.

Bello, A.M., Usman, M.B., Ismail, M.A., Mukkafa, S., Abubakar, U., Kwami, I.A., Al-Ramadan, K., Amao, A.O., Al-Hashem, M., Salisu, A.M., Kachalla, A., Abubakar, M.B., Maigari, A. S., & Chiroma, L.U., 2023. Linking diagenesis and reservoir quality to depositional facies in marginal to shallow marine sequence: An example from the Campano-Maastrichtian Gombe Sandstone, Northern Benue Trough, NE Nigeria. Marine and Petroleum Geology, 155. https://doi.org/10.1016/j.marpetgeo.2023.106386.

Boukhalfa, K., Soussi, M., Reynaud, J.-Y., & Banerjee, S., 2025. Sandstones and red beds in the Lower Cretaceous Sidi Aich Formation, Chotts Basin (Southern Tunisia): facies, architecture and depositional environments. Geological Society, London, Special Publications, 545(1). https://doi.org/10.1144/sp545-2023-181.

Busch, B., Böcker, J., & Hilgers, C., 2024. Improved reservoir quality assessment by evaluating illite grain coatings, quartz cementation, and compaction – Case study from the Buntsandstein, Upper Rhine Graben, Germany. Geoenergy Science and Engineering, 241(8), 213141. https://doi.org/10.1016/j.geoen.2024.213141.

Cao, R., Knapp, J., Bikkina, P., & Esposito, R., 2021. CO_2 Storage Potential Reconnaissance of the Newly Identified Red Beds of Hazlehurst in the Southeastern United States. Frontiers in Energy Research, 9, 793300. https://doi.org/10.3389/fenrg.2021.793300.

Cavaroc, V.V., & Flores, R.M., 1990. Red beds of the Triassic Chugwater Group, southwestern Powder River Basin, Wyoming. US Geological Survey Bulletin, 19, E1-E17.

Chakraborty, R., Tham, M., Sazykin, A., Menzel-Jones, G., Miller, P., Tu, C., Barlass, D., & Adelman, N., 2020. A case study on the largest exploration survey in asia: unlocking the hydrocarbon potential of frontier areas, Offshore Sabah, Malaysia. Offshore Technology Conference Asia 2020, OTCA 2020. https://doi.org/10.4043/30269-ms.

Chima, P., Baiyegunhi, C., Liu, K., & Gwavava, O., 2018. Diagenesis and rock properties of sandstones from the Stormberg Group, Karoo Supergroup in the Eastern Cape Province of South Africa. Open Geosciences, 10(1), 740–771. https://doi.org/10.1515/geo-2018-0059.

Chung, K.W.E.I., Mohamed, K.R., Ali, C.A., Dzulkafli, M.A., & Talib, J.A.B., 2023. The Mangking Sandstone Formation of Kuala Tahan to Kampung Bantal: Sedimentology and Depositional Environment. Sains Malaysiana, 52(11), 3027–3044. https://doi.org/10.17576/jsm-2023-5211-02.

Collins, D.S., Johnson, H.D., & Baldwin, C.T., 2020. Architecture and preservation in the fluvial to marine transition zone of a mixed-process humid-tropical delta: Middle Miocene Lambir Formation, Baram Delta Province, north-west Borneo. Sedimentology, 67(1), 1–46. https://doi.org/10.1111/sed.12622.

Cook, J.E., Goodwin, L.B., & Boutt, D. F., 2011. Systematic diagenetic changes in the grain-scale morphology and permeability of a quartz-cemented quartz arenite. AAPG Bulletin, 95(6), 1067–1088. https://doi.org/10.1306/11151010009.

Dorothy, C., 1970. Clay minerals: A guide to their x-ray identification. Geological Society of America, California. 89 p.

Favoreto, J., Borghi, L., Valle, B., Nunes, M., Santos, H., Arena, M., Lima, M.C.O., Dal' Bó, P.F., Santos, J., Ribeiro, C., Coelho, P., & Mendes, M., 2022. Diagenetic characterization and the influence on the porosity properties of a mixed bioclastic-siliciclastic rift lacustrine deposit of the Sergipe-Alagoas Basin, northeastern Brazil. Marine and Petroleum Geology, 146, 105925. https://doi.org/10.1016/j.marpetgeo.2022.105925.

Franke, W., & Paul, J., 1980. Pelagic redbeds in the Devonian of Germany - deposition and diagenesis. Sedimentary Geology, 25(3), 231–256. https://doi.org/10.1016/0037-0738(80)90043-3.

Freiburg, J.T., Ritzi, R.W., & Kehoe, K.S., 2016. Depositional and diagenetic controls on anomalously high porosity within a deeply buried CO_2 storage reservoir—The Cambrian Mt. Simon Sandstone, Illinois Basin, USA. International Journal of Greenhouse Gas Control, 55, 42–54. https://doi.org/10.1016/j.ijggc.2016.11.005.

Fu, Q., Hu, S., Xu, Z., Zhao, W., Shi, S., & Zeng, H., 2020. Depositional and diagenetic controls on deeply buried Cambrian carbonate reservoirs: Longwangmiao Formation in the Moxi–Gaoshiti area, Sichuan Basin, southwestern China. Marine and Petroleum Geology, 117, 104318. https://doi.org/10.1016/j.marpetgeo.2020.104318.

Garzanti, E., 2019. Petrographic classification of sand and sandstone. Earth-Science Reviews, 192, 545–563. https://doi.org/10.1016/j.earscirev.2018.12.014.

Glad, A.C., Willumsen, M.E., Boldreel, L.O., & Clemmensen, L.B., 2019. Meandering river deposits in sediment cores, the middle jurassic alma field, Southern Danish central graben. Bulletin of the Geological Society of Denmark, 66, 189–209. https://doi.org/10.37570/bgsd-2018-66-10.

Harbury, N.A., Jones, M.E., Audley-Charles, M.G., Metcalfe, I., & Mohamed, K.R., 1990. Structural evolution of Mesozoic Peninsular Malaysia. Journal of the Geological Society, 147(1), 11–26. https://doi.org/10.1144/gsjgs.147.1.0011.

Heald, M.T., & Larese, R.E., 1974. Influence of Coatings on Quartz Cementation. SEPM Journal of Sedimentary Research, 44(4), 1269-1274. https://doi.org/10.1306/212f6c94-2b24-11d7-8648000102c1865d.

Hosa, A., & Wood, R., 2020. Order of diagenetic events controls evolution of porosity and permeability in carbonates. Sedimentology, 67(6), 3042–3054. https://doi.org/10.1111/sed.12733.

Kamp, P.C., & James, R.S., 2022. Origin and Provenance of Archean Keewaywin Formation clastic rocks at Sandy Lake, NW Ontario, Canada: Constraints on Archean weathering and depositional processes. Precambrian Research, 378, 106607. https://doi.org/10.1016/j.precamres.2022.106607.

Khoo, H.P., 1977. Geology of the Sungai Tekai area. Geological Survey of Malaysia Annual Report, 1977, 93-103.

Khoo, H.P., 1983. Proceedings of the Workshop on Stratigraphic Correlation of Thailand and Malaysia, Vol. 1, Technical Papers.

Koopmans, B.N., 1968. The Tembeling Formation - a litho-stratigraphic description (West Malaysia). Bulletin of the Geological Society of Malaysia, 1, 223–243. https://doi.org/10.7186/bgsm01196703.

Krynine, P.D., 1948. The Megascopic Study and Field Classification of Sedimentary Rocks. The Journal of Geology, 56(2), 130–165. https://doi.org/10.1086/625492.

Li, H., Du, X., Wang, Q., Yang, X., Zhu, H., & Wang, F., 2020. Formation of abnormally high porosity/permeability in deltaic sandstones (Oligocene), Bozhong depression, offshore Bohai Bay Basin, China. Marine and Petroleum Geology, 121, 104616. https://doi.org/10.1016/j.marpetgeo.2020.104616.

Lucero, D., Bailey, L., Kim, J. H., Voller, V., Hughes, A., Krantz, R., Lingrey, S., Barton, M. D., Barton, I., Reiners, P., McIntosh, J., Neuzil, C., Thorson, J., & Person, M., 2025. Influence of internal fluid driving mechanisms on red bed bleaching in the Paradox Basin (Colorado Plateau, Utah and Colorado, USA). Bulletin of the Geological Society of America, 137(5–6), 2765–2783. https://doi.org/10.1130/B37654.1.

Madon, M., 2021. Five decades of petroleum exploration and discovery in the Malay Basin (1968-2018) and remaining potential. Bulletin of the Geological Society of Malaysia, 72, 63–88. https://doi.org/10.7186/bgsm72202106.

McKinley, J.M., Worden, R.H., & Ruffell, A.H., 1999. Smectite in Sandstones: A Review of the Controls on Occurrence and Behaviour During Diagenesis. In: Richard H. Worden & Sadoon Morad (Eds.), Clay Mineral Cements in Sandstones. International Association of Sedimentologists, California. 109–128. https://doi.org/10.1002/9781444304336.ch5.

Metcalfe, I., 2013. Tectonic evolution of the Malay Peninsula. Journal of Asian Earth Sciences, 76, 195–213. https://doi.org/10.1016/j.jseaes.2012.12.011.

Miall, A.D., 1985. Architectural-element analysis: A new method of facies analysis applied to fluvial deposits. Earth Science Reviews, 22(4), 261–308. https://doi.org/10.1016/0012-8252(85)90001-7.

Monsees, A.C., Busch, B., & Hilgers, C., 2021. Compaction control on diagenesis and reservoir quality development in red bed sandstones: a case study of Permian Rotliegend sandstones. International Journal of Earth Sciences, 110(5), 1683–1711. https://doi.org/10.1007/s00531-021-02036-6.

Morad, S., Al-Ramadan, K., Ketzer, J.M., & De Ros, L.F., 2010. The impact of diagenesis on the heterogeneity of sandstone reservoirs: A review of the role of depositional fades and sequence stratigraphy. American Association of Petroleum Geologists Bulletin, 94(8), 1267–1309. https://doi.org/10.1306/04211009178.

Morad, S., Ketzer, J.M., & De Ros, L.R., 2000. Spatial and temporal distribution of diagenetic alterations in siliciclastic rocks: Implications for mass transfer in sedimentary basins. Sedimentology, 47(SUPPL. 1), 95–120. https://doi.org/10.1046/j.1365-3091.2000.00007.x.

Ng, S.W.P., Whitehouse, M.J., Searle, M.P., Robb, L.J., Ghani, A.A., Chung, S.L., Oliver, G.J. H., Sone, M., Gardiner, N. J., & Roselee, M.H., 2015. Petrogenesis of Malaysian granitoids in the Southeast Asian tin belt: Part 2. U-Pb zircon geochronology and tectonic model. Bulletin of the Geological Society of America, 127(9–10), 1238–1258. https://doi.org/10.1130/B31214.1.

Ngah, K., Tjia, H.D., Muhamad, A.J., Ali, M.Y., Som, M.R.M., Kong, L.K., & Jirin, S., 1993. Petroleum Potential of the Tembeling Group. Warta Geologi, 6, 19.

Oluwadebi, A.G., Taylor, K.G., & Dowey, P.J., 2018. Diagenetic controls on the reservoir quality of the tight gas Collyhurst Sandstone Formation, Lower Permian, East Irish Sea Basin, United Kingdom. Sedimentary Geology, 371, 55–74. https://doi.org/10.1016/j.sedgeo.2018.04.006.

Otofuji, Y. ichiro, Moriyama, Y.T., Arita, M.P., Miyazaki, M., Tsumura, K., Yoshimura, Y., Shuib, M.K., Sone, M., Miki, M., Uno, K., Wada, Y., & Zaman, H., 2017. Tectonic evolution of the Malay Peninsula inferred from Jurassic to Cretaceous paleomagnetic results. Journal of Asian Earth Sciences, 134, 130–149. https://doi.org/10.1016/j.jseaes.2016.10.007.

Pettijohn, F.J., Potter, P.E., & Siever, R., 1974. Sand and Sandstone. Soil Science, 117(2), 130. https://doi.org/10.1097/00010694-197402000-00013.

Qian, W., Sun, Q., Jones, S. J., Yin, T., Zhang, C., Xu, G., Hou, G., & Zhang, B., 2022. Diagenesis and controlling factors of Oligocene Huagang Formation tight sandstone reservoir in the south of Xihu sag, the East China Sea Shelf Basin. Journal of Petroleum Science and Engineering, 215, article id. 110579. https://doi.org/10.1016/j.petrol.2022.110579.

Qiao, J., Zeng, J., Jiang, S., & Wang, Y., 2020. Impacts of sedimentology and diagenesis on pore structure and reservoir quality in tight oil sandstone reservoirs: Implications for macroscopic and microscopic heterogeneities. Marine and Petroleum Geology, 111, 279–300. https://doi.org/10.1016/j.marpetgeo.2019.08.008.

Reed, F.S., & Mergner, J.L., 1953. Preparation of Rock Thin Sections. Amer. Mineral., 38, 1184–1203.

Robertson, J., Thomas, C.J., Caddy, B., & Lewis, A.J.M., 1984. Particle size analysis of soils - A comparison of dry and wet sieving techniques. Forensic Science International, 24(3), 209–217. https://doi.org/10.1016/0379-0738(84)90186-5.

Shahrokhi, S., Bábek, O., Mansurbeg, H., Ackerman, L., Šimíček, D., Gregar, F., & Kořenek, M., 2024. Investigating the impact of paleoclimatic conditions and diagenesis on the genesis of Permian Continental Red Beds: A case study from the Bohemian Massif, Czechia. Sedimentary Geology, 470. https://doi.org/10.1016/j.sedgeo.2024.106723.

Turner, P., 1980. Chapter 6 The Mineralogy and Geochemistry of Iron Oxides in Red Beds. Continental Red Beds, 29, 323–379. https://doi.org/https://doi.org/10.1016/S0070-4571(08)70250-4.

Wadood, B., Khan, S., Wagreich, M., Vennemann, T., Li, H., Ullah, M., & Schöpfer, K., 2024. Diagenetic history and porosity

evolution of the Middle Permian clastic-carbonate mixed system, Indus Basin, Pakistan: Implications for reservoir development. Energy Geoscience, 5(4), 100317. https://doi.org/10.1016/j.engeos.2024.100317.

Wang, G., Chang, X., Yin, W., Li, Y., & Song, T., 2017. Impact of diagenesis on reservoir quality and heterogeneity of the Upper Triassic Chang 8 tight oil sandstones in the Zhenjing area, Ordos Basin, China. Marine and Petroleum Geology, 83, 84–96. https://doi.org/10.1016/j.marpetgeo.2017.03.008.

Wang, J., Fu, Y., Yan, Z., Fu, J., Xie, J., Li, K., & Zhao, Y., 2021. Influence of sedimentation and diagenesis on reservoir physical properties: a case study of the Funing Formation, Subei Basin, eastern China. Frontiers of Earth Science, 15(4), 892–908. https://doi.org/10.1007/s11707-020-0836-y.

Wilson, M.D., 1992. Inherited Grain-Rimming Clays in Sandstones From Eolian and Shelf Environments: Their Origin and Control on Reservoir Properties. In: Houseknecht, D.W. & Pittman, E.D. (Eds.), Origin, Diagenesis, and Petrophysics of Clay Minerals in Sandstones. SEPM Spec. Publ. 47, 209–225. https://doi.org/10.2110/pec.92.47.0209.

Worden, R.H., & Burley, S.D., 2003. Sandstone Diagenesis: The Evolution of Sand to Stone. In: Stuart D. Burley & Richard H. Worden (Eds.), Sandstone Diagenesis: Recent and Ancient, 1–44. https://doi.org/10.1002/9781444304459.ch.

Worden, R. H., & Utley, J. E. P., 2022. Automated mineralogy (SEM-EDS) approach to sandstone reservoir quality and diagenesis. Frontiers in Earth Science, 10. https://doi.org/10.3389/feart.2022.794266.

Yuan, X., Hu, Q., Fang, X., Wang, Q., Ma, Y., & Tachi, Y., 2024. Archie's cementation factors for natural rocks: Measurements and insights from diagenetic perspectives. Sedimentary Geology, 465, 106633. https://doi.org/10.1016/j.sedgeo.2024.106633.

Manuscript received 5 August 2025;
Received in revised form 20 October 2025;
Accepted 6 January 2026
Available online 27 November 2026